Nucleon Elastic and Transition Form Factors with the CEBAF 12 GeV Upgrade

June 13, 2000

R. Gilman[4,11], P. Stoler[10], A. Afanasev[4,8], A. Ahmidouch[9]
K. Baker[2,4], W. Brooks[4], M. Jones[6], W. Melnitchouk[1,4], A. Nathan[3],
C. Perdrisat[12], G. Petratos[5], V. Punjabi [7], B. Wojtsekhowski[4]

[1] *Center for the Subatomic Structure of Matter, University of Adelaide, Adelaide, Australia*
[2] *Hampton University, Hampton, VA, USA*
[3] *University of Illinois, Urbana-Champaign, IL, USA*
[4] *Jefferson Laboratory, Newport News, VA, USA*
[5] *Kent State University, Kent, OH USA*
[6] *University of Maryland, College Park, MD, USA*
[7] *Norfolk State University, Norfolk, VA, USA*
[8] *North Carolina Central University, NC, USA*
[9] *North Carolina A&T State University Greensboro, NC, USA*
[10] *Rensealler Polytechnic Institute, Troy, NY USA*
[11] *Rutgers University, New Brunswick, NJ, USA*
[12] *College of William and Mary, Williamsburg, VA, USA*

1 Introduction

The nucleon elastic and transition form factors are fundamental quantities in high energy nuclear physics. They are the most basic observables which reflect the composite nature of the nucleon, the defining problem for nuclear physics. Indeed, historically, the first indication that the nucleon is not elementary came from measurements of the form factors in elastic electron–proton scattering [1].

The nucleon spin problem again makes it clear that the nucleon has an interesting nonperturbative structure. The viewpoint of inclusive deep inelastic scattering (DIS), in which only the longitudinal momentum fraction of the partons is important, is clearly not adequate. While there are many possible approaches to describing the nucleon structure, ranging from the constituent quark model and lattice gauge theory at low momentum transfer, to perturbative quantum chromodynamics (pQCD) at very large momentum transfer, it is the framework of generalized parton distributions (GPDs) that is generating excitement. GPDs allow a unified consistent understanding of the elastic, inelastic (resonance), and deep inelastic structure of the nucleon.

For electron and photon scattering, the physical picture in this framework is that the real or virtual photon interacts with a single active quark within the nucleon; the nonperturbative wave function of this active quark within the nucleon is described by the GPDs. This picture of the reaction mechanism, a generalization of the Feynman mechanism, is believed to be dominant at momentum transfers accessible with the CEBAF upgrade. Of particular interest is that exclusive reactions described with GPDs determine the orbital angular momentum contribution of the up, down, and strange quarks to the nucleon spin, complementing the quark spin contributions determined with polarized inclusive DIS. The physical basis for describing the form factor measurements that we propose with GPDs is well established. The proposed measurements will study the t dependence of the GPDs, being particularly sensitive to large transverse momenta within the nucleon.

Measurements of form factors have, of themselves, become more exciting in recent years, due to the precise measurement techniques now available, and the surprising results that have been obtained. At small Q^2, below 1 GeV^2, the neutron charge form factor has finally been determined to be statistically significantly different from 0; the neutron magnetic form factor remains controversial due to disagreements between precise experiments in excess of their stated uncertainties. For the proton, recent Jefferson Lab polarization measurements [2] show, with few percent uncertainties, that the electric form factor falls much faster than the magnetic form factor. This proves that the accepted textbook picture for many years [1], in which these distributions are equal, is wrong.

The goal of this proposal is a precise consistent exploration of several form factors up to momentum transfers of $Q^2 = -t = 10$ - 15 GeV^2. Currently, precise measurements only exist for the magnetic proton form factor above a few GeV^2. The proposed measurements include elastic nucleon form factors, the Δ and S_{11} transition form factors, and real Compton scattering (RCS). Although RCS has not previously been thought of as a form factor experiment, within the GPD framework it measures vector and axial vector form factors, complementing, for example, the vector and tensor measurements of elastic scattering. Baryon resonance structure generalizes the elastic nucleon structure problem and allows deeper insights. Indeed, the resonances provide a bridge between the elastic and deep inelastic regimes. The Δ resonance is significant for its role in hadron structure, and for the qualitatively different Q^2 dependence of its form factor from the elastic and other resonant form factors. The S_{11} resonance is the negative parity partner of the nucleon. These data should lead to a deeper understanding of the nonperturbative structure of the nucleon, and a better understanding of the interrelationships between the elastic, inelastic, and deep inelastic structure of the nucleon. Evidence for the onset of a transition from nonperturbative to perturbative behavior is also possible.

2 Theoretical background

2.1 Conventional description of form factors

The nucleon elastic form factors are defined through matrix elements of the electromagnetic current, $J_\mu = \overline{\psi}\gamma_\mu\psi$, where ψ is a quark field in the nucleon, as:

$$\langle N(P')|J_\mu(0)|N(P)\rangle = \overline{u}(P')\left(\gamma_\mu F_1(Q^2) + \frac{i\sigma_{\mu\nu}q^\nu}{2M}F_2(Q^2)\right)u(P) \ ,$$

where P and P' are the initial and final nucleon four momenta, and $q = P - P'$ is the momentum transferred to the nucleon, with $Q^2 = -q^2 = -t$. The Sachs electric and magnetic form factors are defined in terms of F_1 and F_2 as:

$$G_E(Q^2) = F_1(Q^2) - (Q^2/4M^2)\ F_2(Q^2),$$

$$G_M(Q^2) = F_1(Q^2) + F_2(Q^2) \ .$$

In the Breit frame, in which the energy transfer to the nucleon is zero ($Q^2 = \vec{q}^{\,2}$), the elastic electric and magnetic form factors measure the distributions of charge and magnetization in the nucleon:

$$G_E(Q^2) = \int d^3r \ e^{-i\vec{q}\cdot\vec{r}} \rho_E(r) \ , \tag{1}$$

$$G_M(Q^2) = \int d^3r \ e^{-i\vec{q}\cdot\vec{r}} \rho_M(r) \ . \tag{2}$$

At low Q^2 the distance scales on which the electromagnetic scattering takes place are large, so that the resolving power of the probe is only sufficient to measure the static properties of the nucleon. The nucleon's magnetic moment is given by $G_M(Q^2 = 0) = \mu$, while the charge radius is: $\langle r^2 \rangle = -6 \ dG_E/dQ^2|_{Q^2=0}$. The form factors at low Q^2 are known to approximately follow the dipole form, $G(Q^2) \propto 1/(1 + \frac{Q^2}{Q_0^2})^2$, with $Q_0^2 \approx 0.71$ GeV^2. This behavior corresponds to an exponential distribution in space, but can also be qualitatively understood within a vector meson dominance picture. However, deviations of about 10% from the dipole form have been observed, and it is important to understand the nature of the deviations at larger Q^2.

Resonance form factors can be described very similarly to the elastic form factor description above. At the other extreme of asymptotically large Q^2, these elastic and resonance form factors are expected to be described in terms of perturbative QCD [4]. Here the short wavelength of the highly virtual photon enables the quark substructure of the nucleon to be cleanly resolved. Just where the perturbative behavior sets in is still an open question, which must be resolved experimentally. Evidence from recent experiments at Jefferson Lab and elsewhere suggests that non-perturbative effects are still quite important at least for $Q^2 < 10$ GeV^2. For example, one expects asymptotically for the proton form factors that $Q^2 F_2/F_1 \rightarrow$ constant, implying $G_E/G_M \rightarrow$ constant, but G_E/G_M varies strongly with Q^2 at least to 3.5 GeV^2 [2]. In the $N \rightarrow \Delta$ transition, the corresponding quantity, the $E2/M1$ ratio, remains nearly 0 over the entire measured range of momentum transfer, up to 4 GeV^2 [3]. This observation agrees with the constituent quark model, with no observed change towards the perturbative expectation that $E2/M1 \rightarrow 1$.

Understanding the transition from the low to high Q^2 regions is vital not only for determining the onset of perturbative behavior. Form factors in the transition region are very sensitive to mechanisms of spin-flavor symmetry breaking, which cannot be described *in principle* within perturbation theory. A classic example is the electric form factor of the neutron, G_E^n [5], which is identically zero in a simple valence quark picture, and whose non-zero value can only be understood in terms of non-perturbative mechanisms such as the hyperfine interaction between quarks [6], or a pion cloud [7]. Similarly, in the purely asymptotic picture with the symmetric distribution amplitude for the proton, the electric form factor is identically zero. Thus, the nonvanishing electric form factor requires a nonperturbative wave function.

2.2 Generalized Parton Distributions

The information on nucleon structure contained in form factors is complementary to that which is measured through other processes, such as inclusive scattering. Recent work on generalized parton distributions (GPDs), has provided a unifying framework within which both form factors and structure functions can be simultaneously embedded [8, 9]. GPDs describe the non-perturbative process of quark/parton emission and subsequent absorption by a hadron in an exclusive reaction. This picture can be applied to the elastic and resonance transition form factors, to the extent that the momentum transferred to the struck quark is shared with the nucleon through the wave function, rather than through hard gluon exchanges. Indeed, this picture is on a firmer basis for the form factors, in which the photon is absorbed and no particles are emitted, than for processes like the real Compton scattering or meson production. These processes also require the dominance of handbag diagrams; that is, the emitted photon (or meson) must arise from the struck quark before any interaction with the rest of the nucleon.

There are four generalized parton distributions, $\mathcal{F}^q(x,t,\xi)$, $\mathcal{G}^q(x,t,\xi)$, $\mathcal{K}^q(x,t,\xi)$, and $\mathcal{P}^q(x,t,\xi)$, corresponding to vector, axial vector, tensor, and pseudoscalar matrix elements, respectively. Here x is the quark momentum fraction, $t = (P - P')^2$, and $\xi = n \cdot (P' - P)$, with n a light-like vector. Physically, ξ is half of the longitudinal momentum transfer to the struck quark. The superscript q indicates that the GPDs are different for the different quark flavors. The nucleon elastic form factors are given by moments of these distributions summed over quark and anti-quark flavors:

$$F_1(t) = \Sigma_q e_q \int_0^1 dx \mathcal{F}^q(x,t)$$

and

$$F_2(t) = \Sigma_q e_q \int_0^1 dx \mathcal{K}^q(x,t).$$

There is also the axial form factor:

$$G_A(t) = \Sigma_q e_q \int_0^1 dx \mathcal{G}^q(x,t).$$

In the limit of inclusive scattering, the GPDs reduce to the standard parton distributions, with the spin independent momentum distribution

$$q(x) = \mathcal{F}^q(x, t=0, \xi=0)$$

and the polarized momentum distribution

$$\Delta q(x) = \mathcal{G}^q(x, t=0, \xi=0).$$

Thus, one can see the connection between the form factors, given by moments of GPDs, and the inclusive DIS distributions, which are the $t=0, \xi=0$ limits of the GPDs.

While the form factors determine the $< x^0 >$ moments of the GPDs, the RCS cross section determines the $< x^{-1} >$ moments. Neglecting small corrections arising from $\mathcal{K}^q(x,t,\xi)$, it is written in terms of two form factors,

$$\frac{d\sigma}{d\Omega}_{RCS} = \frac{d\sigma}{d\Omega}_{Klein-Nishina} \times \left[f_V R_V^2(t) + (1-f_V) R_A^2(t) \right]$$

with the kinematic factor f_V given by

$$f_V = \frac{(s-u)^2}{2((s-m^2)^2 + (u-m^2)^2)},$$

and the RCS form factors given by:

$$R_V(t) = \Sigma_q e_q^2 \int_0^1 dx \frac{\mathcal{F}^q(x,t)}{x}$$

and

$$R_A(t) = \Sigma_q e_q^2 \int_0^1 dx \frac{\mathcal{G}^q(x,t)}{x}.$$

While the elastic form factors at large t become increasingly sensitive to high x, RCS remains sensitive to small x due to the $1/x$ weighting in the integral. The kinematic factor f_V always tends to be large, near 1, leading to sensitivity mainly for R_V. Sensitivity to R_A is obtained by measuring the longitudinal polarization transfer from the photon to the proton:

$$A_{LL}\frac{d\sigma}{dt} \equiv \frac{d\sigma(\uparrow\uparrow)}{dt} - \frac{d\sigma(\uparrow\downarrow)}{dt}$$

In terms of the form factors,

$$A_{LL}\frac{d\sigma}{d\sigma_{\rm KN}} = A_{LL}^{\rm KN} R_V(t) R_A(t),$$

allowing R_A to also be determined.

The different charge weightings of e_q^2 in the RCS form factors versus e_q in the elastic form factors, plus measurements on the proton and neutron, provides flavor sensitivity. Also, the various reaction processes yield information on helicity flip versus helicity conserving amplitudes. We can access this information by determining the elastic Dirac and Pauli form factors F_1 and F_2. In the $N \to \Delta$ transition, this is seen through the ratio $E2/M1$. For RCS, the combination $|R_V + R_A|^2$ gives the probability that the nucleon and struck quark have the same helicity, while the combination $|R_V - R_A|^2$ gives the probability that the nucleon and struck quark have the opposite helicity. Thus, the spin structure of the form factors can be determined.

GPDs allow the initial and final hadronic states involved in the reaction to be different; this allows sensitivity to the orbital angular momentum of quarks and was the original motivation of Ji to introduce this formalism [8]. The Angular Momentum Sum Rule relates the first moment of GPDs in the forward limit to the total angular momentum of quarks and gluons, with orbital angular momentum *included*. For the case of quarks it reads

$$J_q = \frac{1}{2}[A_q(0) + B_q(0)],$$

where

$$A_q(t) = \int_0^1 dx x \mathcal{F}^q(x,t,\xi)$$

and

$$B_q(t) = \int_0^1 dx x \mathcal{K}^q(x,t,\xi),$$

neglecting terms that do not contribute to the Angular Momentum Sum Rule. It demonstrates that the form factors that we propose to measure here

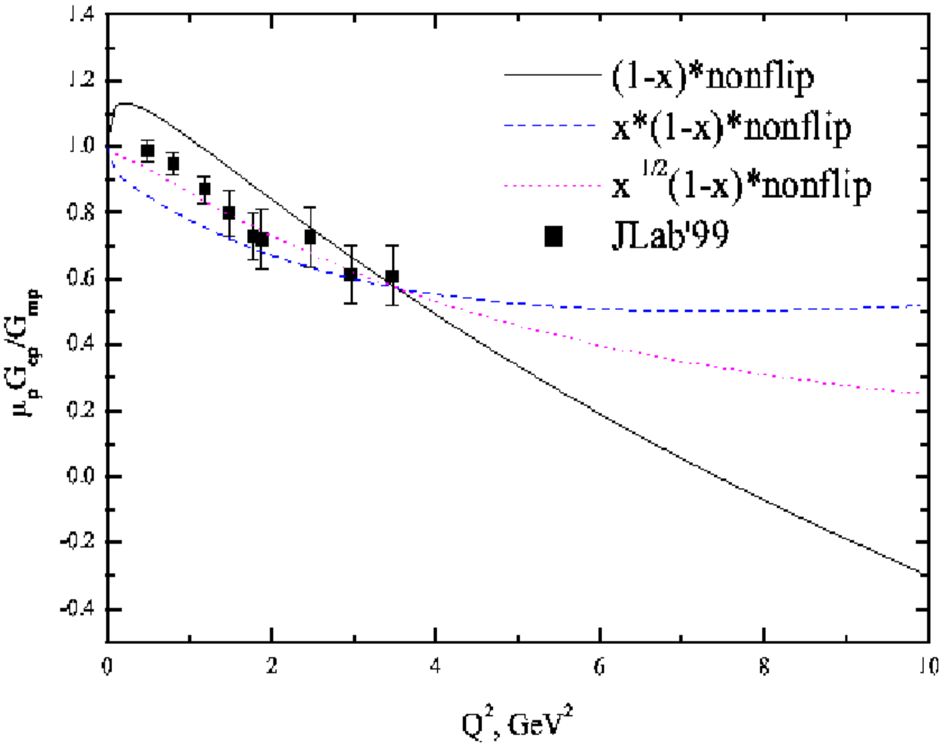

Figure 1: Recent Jefferson lab polarization results [2] for $\mu G_E^p/G_M^p$ compared to a GPD model [11], with three different assumptions for the form of the relation between the tensor and vector (nonflip) GPDs, $\mathcal{K}$ and $\mathcal{F}$. The calculations are valid for Q^2 above 1 or 2 GeV^2.

are in fact closely related to the problem of nucleon spin in the quark-parton framework, as they involve different moments $< x^n >$ of the GPDs.

In recent theoretical developments, the t-dependence of GPDs has been modeled in a study of both Dirac [10] and Pauli [11] form factors of the proton. We give an explicit example: the vector GPD that lead to the Dirac form factor F_1 is modeled as

$$\mathcal{F}^q(x,t) = q^q(x) e^{(1-x)t/4x\lambda^2},$$

with $q^q(x)$ the standard parton distribution taken from published fits, and λ a parameter that determines the characteristic transverse momentum in the nucleon. The Pauli form factor arises from the tensor GPD, which has a similar form to the vector GPD given above, with additional powers of x. Three parameterizations were tried, as shown in Fig. 1. Using the relations given above, these GPD models can be used to estimate the contribution of the quarks to the proton spin. Afanasev [12], using the fits to the G_E^p/G_M^p data of JLab E93-027 [2] shown in Fig. 1, concluded that about 50% of the nucleon spin comes from the orbital angular momentum plus spin contributions of the valence quarks. This result changes by only a few percent between the different parameterizations tried.

The power of the GPD formalism is that it allows a universal description of handbag-type diagrams involving current quarks. In particular, the same GPD of a nucleon would describe nucleon elastic and resonance form factors, real and virtual Compton scattering, and hard electro- and photoproduction of mesons on the nucleon. Different experiments would cover different regions of the three kinematic variables characterizing GPDs. In particular, as factorization has been proven for hard meson electroproduction at low $-t$, these experiments largely map out the x dependence of the GPDs at low $-t$. The form factor measurements proposed here provide a complementary investigation of the t dependence of some of the $< x^n >$ moments.

Importantly, the intrinsic transverse momentum of the partons is crucial for determining the $-t = Q^2$ dependence of the form factors. Therefore the problem becomes related, for instance, to the problem of single–spin asymmetries in semi-exclusive hadronic and leptonic scattering (see [13] and references therein). As the form factor measurements continue to higher t, there is increasing sensitivity to large intrinsic transverse momenta, as well as to the high Bjorken x valence quark region, relative to the low x sea quark region. This can be seen from the equation for $\mathcal{F}^q(x,t)$ given above.

Examination of the GPD calculation [10] compared to the data indicates that for t above about 5 GeV^2, the calculation decreases faster than the data, possibly indicating the need for hard correlated processes - that is, quark-quark correlations due to gluon exchange to generate additional strength at large transverse momenta. The soft Gaussian dependence shown above may be modified by additional correlation terms, and one may expect the formula above to become of the form:

$$\mathcal{F}^q(x,t) = q^q(x)\left[e^{(1-x)t/4x\lambda^2} + \Sigma_n c_n \frac{(\alpha_s/\pi)^{2n}}{t^{2n}}\right],$$

These correlation terms can only be sampled at large t, after the Gaussian has fallen off. Sensitivity to these correlations is a unique feature of these proposed measurements.

2.3 Duality

From another perspective, the interplay between elastic and resonance form factors and structure functions is central to the phenomenon of quark-hadron duality [14, 15, 16, 17, 18], and the transition from quark to hadron degrees of freedom in QCD. These form factors obtained in exclusive reactions can be related through local quark-hadron duality to deep-inelastic structure functions measured in inclusive processes, at the corresponding values of x and Q^2. The elastic form factors for example can be used to predict the behavior of structure functions in the limit $x \to 1$ [14, 19, 20, 21]. It is in general difficult to experimentally access the large x, large W DIS region, but duality allows estimates to be made from the more experimentally accessible resonance data at large x and small W. As an example, the DIS structure function F_1 of the nucleon is related to the elastic magnetic form factor at large Q^2 through [14, 21]:

$$F_1(x \to 1, Q^2) \;\propto\; \frac{dG_M^2(Q^2)}{dQ^2}\ . \tag{3}$$

Conversely, from data on structure functions at very large x one can extract the form factors as a function of Q^2 and compare with the directly measured values [15, 16].

One can similarly use quark-hadron duality to study not just the elastic case, but the entire spectrum of excited final states, and more generally the transition from resonance production to scaling in deep-inelastic scattering [22]. The form factors which parameterize transitions from the ground state to the excited states, such as $N \to \Delta$ or $N \to S_{11}$, contain rich information about the spatial distribution of quarks inside the nucleon.

The $N \to \Delta$ transition form factor is particularly important given the prominent role that the Δ is known to play in hadron structure [7]. The previously observed Q^2 dependence of the $\gamma^* N\Delta$ form factor is qualitatively different from the Q^2 dependence of the form factors of the other resonances [23]. Moreover, the contribution of the $N \to \Delta$ transition to the polarization asymmetry

$$A_1 = \frac{\sigma_{1/2} - \sigma_{3/2}}{\sigma_{1/2} + \sigma_{3/2}} , \tag{4}$$

where $\sigma_{1/2(3/2)}$ is the virtual photoabsorption cross section for total γ^*-nucleon spin projection 1/2 (3/2), is known to be large and negative at low Q^2, while the same asymmetry at large Q^2 is positive. Understanding this transition, and the related non-trivial Q^2 dependence of the Gerasimov-Drell-Hearn sum rule at intermediate Q^2, requires a precise determination of the $\gamma^* N\Delta$ form factor over a large range of Q^2. (However, while the Δ makes a large contribution to the sum rule at small Q^2, its contribution at large Q^2 is small compared to that of the DIS region.)

The next lowest strongly excited state after the Δ is the negative parity partner of the nucleon, the S_{11} resonance. In the limit of exact chiral symmetry, the masses of the nucleon and its parity partner would be degenerate, so that the properties of the S_{11} form factor reveal fundamental aspects of dynamical chiral symmetry breaking in QCD.

2.4 Theory Summary

We have indicated above that the generalized nucleon form factors are interesting objects in and of themselves, describing an aspect of the internal structure of the nucleon. These quantities are related to exclusive and deep inelastic reactions within the framework of generalized parton distributions, and also by quark hadron duality. The evolution of the form factors from the nonperturbative to perturbative regimes, and from the elastic ($x = 1$) to the deep inelastic ($x << 1$) regimes, are fundamental questions for nuclear physics. The measurements proposed here will have an impact on our knowledge of the internal structure of the nucleon, specifically on topics such as the orbital angular momentum and the large transverse momentum distribution of quarks in the nucleon, topics that are otherwise difficult to access.

Recently, a new generation of experiments has allowed precise determinations of these quantities at low Q^2, below 1 GeV^2, in most cases, and to Q^2 of a few GeV^2 in some cases. With the CEBAF 12 GeV upgrade, it is possible to extend *precise* form factor measurements to $Q^2 \approx 15$ GeV^2 in most cases, significantly extending the range and quality of existing data. In the following sections, we describe the proposed measurements of the form factors.

3 The Measurements

We propose to measure the nucleon elastic form factors, G^n_M, G^p_E, G^p_M, the transition form factors for $N \to \Delta$ and $N \to S_{11}$, and wide angle RCS. All of these proposed measurements can be carried out to large Q^2, ≈ 15 GeV^2, with good precision. Notably missing from these measurements is the neutron electric form factor, for which measurements with current technology appear to be limited to about 2 GeV^2. The proposed measurements are discussed in detail in the following sections.

3.1 The proton electric form factor

The first precise measurement of G^p_E/G^p_M to 3.5 GeV^2 in Hall A [2] has shown markedly different Q^2 dependences for G_{Ep} and G_{Mp}. This was very surprising in light of existing data [24], which showed very similar Q^2 dependences for these two form factors. However, previously, G_{Ep} was not well defined above Q^2=1 GeV^2. Theoretically, while this difference had not really been predicted, specific features of quark based, as well as mesonic based models can probably account for it. One of the most interesting outstanding questions now is, of course, what is Q^2 dependence of G_{Ep} beyond 3.5 GeV^2.

Here we first show that with an 11 GeV beam it will be possible to measure G^p_E/G^p_M up to $Q^2 \approx 14$ GeV^2 by the recoil polarization technique used in Jlab experiment 93-027 [2]. As the pp scattering analyzing power is zero near T_p=16 GeV, the absolute limit of the recoil polarization method is $Q^2 \approx 28$ GeV^2. Practically, the limit may be $A_y^{pp} \sim 0.1$, which occurs near T_p=9 GeV, corresponding to 17 GeV^2.

Measurements could be done with the existing Hall C HMS spectrometer up to $Q^2 \approx 12$ GeV^2, but the accelerator upgrade is best exploited for these measurements with a corresponding instrumentation upgrade: a medium-resolution, medium-acceptance, 8.5-GeV/c spectrometer is needed. The proposed Medium Acceptance Device (MAD) for Hall A has a baseline design close to the needs of this measurement, with a solid angle twice as large as needed, but a maximum central momentum that needs to be increased.

In Fig. 2 we demonstrate that $Q^2 = 14$ GeV^2 is actually the highest value which can be measured with an 11 GeV beam from the point of view of optimizing the G_E^p/G_M^p error bar over time: the statistical uncertainty reaches its minimum at 11 GeV, and then increases slowly. This fact is independent of actual analyzing power, beam intensity and helicity, and detector solid angles, as long as the electron solid angle is matched to the proton solid angle. The absolute uncertainty scale Fig. 2 makes several reasonable assumptions and extrapolations about available luminosities, spectrometers, polarimeter performance, and run times, but some of these parameters are not well controlled, and ultimate performance will probably differ; these issues are addressed further below.

3.1.1 Kinematics

The kinematics for three typical data points which would become measurable with an 11 GeV beam are shown in Table 1. The rate is calculated for a current of 100 μA on a 15-cm long LH_2 target, and with a 16 msr solid angle spectrometer.

A new spectrometer is assumed. It must analyze protons up to 8.5 GeV/c, and should have a solid angle of approximately 16 msr. An angular resolution of 1-2 mr both horizontally and vertically is required, taking into account the use of an extended target. The angular resolution affects mainly the systematic uncertainty on the precession angle of the proton magnetic moment in the dipole. The full spin rotation correction can be applied using the technique developed for experiment 93-027 in Hall A.

Kinematic matching of the electron arm to the hadron arm is needed. This can be achieved with a calorimeter consisting of an array of lead glass shower detectors; a calorimeter with active an area of $\sim$2.0-3.0 m^2 located at 4 to 5 meters from the target can maintain kinematical matching up to Q^2=14 GeV^2. The granulation of this detector has to be such that a stand-alone angular resolution of $\leq$ 2mr (1σ) can be obtained off-line (for point target). Our recent test runs in Hall A with a 1 m^2 calorimeter indicates

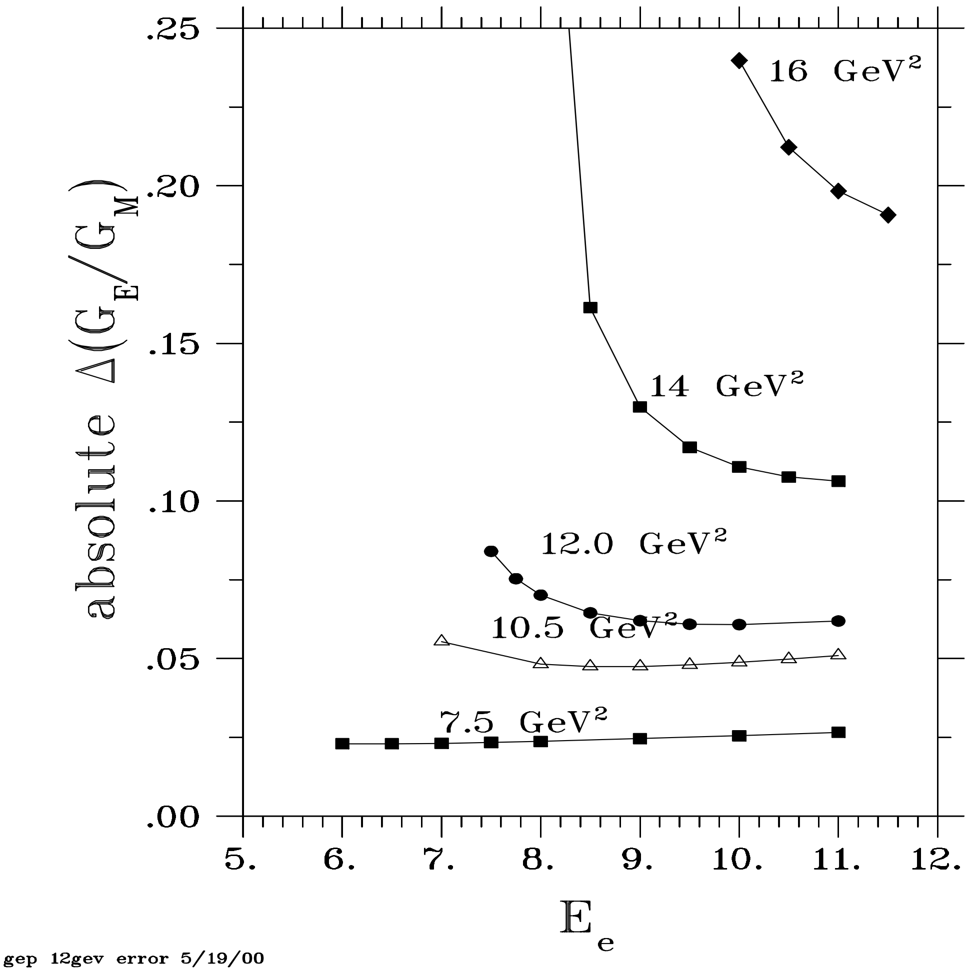

Figure 2: Estimated statistical error bars versus beam energy for the 3 new values of Q^2 proposed, and the control point at 7.5 GeV^2. $Q^2 = 16$ GeV^2 has been included to show that it is probably out of range. Kinematic matching is assumed for each point.

that these numbers are all reasonable.

The analyzing power of the polarimeter does not need to be known in advance to obtain G_E^p/G_M^p; it is calibrated by the experiment. However, the analyzing power directly affects the size of the statistical uncertainties, so these can only be roughly estimated until the experiment is run. The proton energy (momentum) corresponding to $Q^2 = 14$ GeV^2 is 7.5 GeV (8.5 GeV/c). We do not currently have reliable predictions for the analyzing power for protons of energy larger than 5 GeV. Therefore, estimates of the size of error bars which could be obtained for $Q^2 \geq 9$ GeV^2 are not entirely reliable at this time. Currently the largest proton energy for which we have graphite analyzing power data is 2.4 GeV, and we rely on Monte Carlo estimates for higher energies.

After completion of E99-007, scheduled for Jefferson Lab Hall A in November 2000, it will become possible to make a more reliable estimate of the time required to measure the 3 new data points in Table 1, at $Q^2 = 10.5$, 12.0 and 14 GeV^2, and the control point at 7.5 GeV^2. The control point coincides with one of the data points being proposed to PAC 18 for a measurement in Jefferson Lab Hall C. This proposal includes a CH_2 analyzer of 120 cm thickness and requests measurements of the proton electric form factor that will also extend knowledge of the analyzing power of CH_2 to 4.8 GeV ($Q^2 =$ 9 GeV^2). These measurements, possible in the next few years, would further serve to put the extension of the G_E^p/G_M^p ratio on a firmer basis.

Q^2 GeV^2	E_e GeV	θ_e deg	$E_{e'}$ GeV	θ_p deg	p_p GeV/c	$d\sigma/d\Omega_e$ cm^2/sr	χ deg	$\Delta\Omega_e$ msr	rate Hz
7.5	6.6	43	2.2	18	4.84	1.3×10^{-36}	165	80	44
10.5	8.8	40	2.7	16	6.47	3.8×10^{-37}	218	94	12
12	11.0	32	4.1	17	7.27	3.5×10^{-37}	245	52	7
14	11.0	38	3.0	13	8.35	7.6×10^{-38}	280	125	4

Table 1: Kinematics proposed; the assumed beam intensity and polarization are 100 μA and 0.8, respectively.

To summarize, the proton electric form factor G_E^p can be precisely measured up to a momentum transfer of $Q^2 = 14$ GeV^2. The requirements include an 8.5 GeV/c spectrometer with approximately 16 msr solid angle, a vertical bending angle near 17.5°, good angle resolution of 1-2 mr, and modest momentum resolution (0.001-0.01), plus a large calorimeter (about 2-3 m^2 area) with granularity 4 cm. Reliable estimates of times required will have to await completion of 2 experiments, E99-007 scheduled for Hall A in Nov. 2000, and a new experiment proposed to PAC 18 for Hall C.

3.2 The proton magnetic form factor

The proton magnetic form factor has been measured with Rosenbluth separations [24] up to a four momentum transfer of 8.8 GeV^2, and with unseparated cross sections [25] under the assumption that $G_E = G_M/\mu_p$ up to a four momentum transfer of 31 GeV^2. These measurements have precisions of $\approx$ 2-3% out until about Q^2 of 15 GeV^2, then grow to $\approx$ 10% by Q^2 of 31 GeV^2. However, the recent Jefferson lab G_E^P data [2] call into question both the accuracy of the Rosenbluth separations at the lower Q^2, and the dipole assumption at the higher Q^2.

In Table 2, we present, for selected points from the high Q^2 data of [25], calculations of what percentage of the cross section is due to the electric form factor. These data were taken at forward angles, between 21 and 33°. The dipole estimate, used by [25], assumes $\mu G_e^P = G_M^p$. The Bosted estimate is based on a parameterization of the data [26]; the fit was dominated at high Q^2 by the cross sections of [25] and by the separations of [24]. The JLab G_E^p estimate uses the dipole form factor for the magnetic form factor, and assumes that G_E^p/G_D falls linearly with Q^2, as has been seen up to Q^2 of 3.5 GeV^2 in the Jefferson Lab Hall A polarization data.

The point of this exercise is that the electric form factor can make a significant contribution to the forward angle, large Q^2 cross sections. Even within the limited range of assumptions tried here, the undetermined G_E^p dominates the uncertainties in the G_M^p measurement,, and these determinations cannot be fully trusted. Clearly, these data can be reanalyzed once new G_E^p measurements are made, but these polarization measurements can only be made for a limited number of kinematic points, due to the large statistics required. Here, we propose to measure cross sections for a larger set of kinematic points, using lower energies and larger scattering angles than had been done at SLAC, to emphasize the magnetic form factor, putting its determination on a firmer basis. Note that the situation is even more critical for extraction of F_1^P, since naive estimates indicate that while G_E^P is a few percent contribution to the cross section, F_2^P has two to three times as large a contribution to the cross section.

Table 2: Estimated contribution of the electric form factor to selected G_M^P data points at large Q^2, for three different models for the Q^2 dependence of G_E^p. The actual values of G_E^p could be far different from any of these models.

Q^2 (GeV^2)	dipole	Bosted	JLab G_E^p
3.6	9.4	10.0	4.1
7.3	4.9	7.4	0.4
15.7	2.0	5.6	0.7

Here we assume a 100 μA beam incident upon a 15 cm long cryogenic LH_2 target. While the existing Hall A HRS spectrometer could be used for these measurements, the larger solid angle of the proposed MAD spectrometer is assumed, as it allows the measurements to be done in significantly less time. Coincidence detection of the proton is not needed. We demonstrate in Table 3 that a series of short measurements allows us to easily and precisely span a large kinematic range of Q^2 with the accelerator upgrade. The kinematically allowed maximum Q^2 with 11 GeV beam is just below 20 GeV^2, and the measurements require only short times up to $Q^2 = 18$ GeV^2. The estimated contribution from the electric form factor, *assuming the dipole parameterization*, is about 1% in these kinematics, typically a factor of several smaller than for the SLAC measurements.

Table 3: Proposed kinematics for G_M^p measurements.

Q^2 (GeV^2)	E_e (GeV)	θ_e (deg)	E'_e (GeV)	rate (/hr)	statistics (%)	time (days)
10	6.63	65.	1.31	1886	1.4	0.1
11	7.19	65.	1.33	1094	1.4	0.2
12	7.74	65.	1.34	661	1.4	0.3
13	8.29	65.	1.36	414	1.4	0.5
14	8.83	65.	1.37	268	1.8	0.5
15	9.38	65.	1.39	178	1.5	1.0
16	9.92	65.	1.40	120	1.9	1.0
17	10.47	65.	1.41	84	1.8	1.5
18	11.00	65.	1.42	60	1.9	2.0

3.3 The neutron magnetic form factor

It is important to measure both proton and neutron elastic form factors, due the underlying theoretical relations between them. Because the neutron charge form factor is likely to be very small at higher Q^2, the neutron magnetic form factor gives the only information on the quark currents in this system. However, there is currently no microscopic model which successfully predicts both proton and neutron form factors in the non-perturbative domain over a wide range in Q^2. Measurements closer to the region of validity of pQCD will help to shed light on the nature of the failures of these models, facilitating extension of our understanding from the simpler high-Q regime to the more complex world of constituent quarks and gluon flux tubes. The only existing precise measurements of G_M^n, for Q^2 below 1 GeV^2 [27], are somewhat inconsistent; extractions of G_M^n at larger Q^2 are both imprecise and model dependent [26, 28]. An 11 GeV beam enables precision measurements of the neutron magnetic form factor to unprecedentedly small distance scales, more than tripling the Q^2 coverage of the world's data in the important transition region, from nonperturbative QCD to pQCD, where the GPDs are expected to apply.

3.3.1 Experimental Aspects

The measurement discussed here is a a straightforward extension of experiment Jefferson Lab Hall B E94-017, a precise determination of the neutron magnetic form factors from $Q^2 = 0.2$-$4.8\ \ GeV^2$. This measurement was performed in the CEBAF Large Acceptance Spectrometer (CLAS) at Jefferson Lab in the Spring of 2000.

The basic procedure is to measure the ratio of electron-neutron scattering to electron-proton scattering in quasielastic kinematics. The ratio of the differential cross sections yields the neutron magnetic form factor, as long as the proton form factors are known.

At high Q^2, the dominant systematic uncertainty in the measurement is due to increased difficulty in suppressing inelastic reactions. The primary selection criteria for quasielastic scattering are cuts on W and on the angle between the virtual photon and the outgoing nucleon. Because of kinematic factors, at high Q^2 the latter distribution becomes very narrow and the W distribution broadens. Because the inelastic cross section is much larger than the quasielastic cross section, additional suppression of the inelastic background is needed. The additional suppression is provided by the multi-particle detection capability of CLAS.

The upgraded CLAS will have a nearly hermetic coverage in the forward direction. Events with additional particles not characterized by quasi-elastic kinematics can be vetoed by the upgraded version of CLAS. A GEANT simulation of the existing CLAS geometry has already demonstrated a significant amount of rejection power due to this 'multi-particle veto'. Increased coverage in the most forward region and within the torus cryostat for both neutrals and charged particles should provide sufficient information to reduce the uncertainty from this effect to less than five percent.

There are a number of other experimental errors which are expected to contribute at a smaller level. Since the proton and the neutron are measured with different detectors, the uncertainty in the definition of their solid angles will contribute a small uncertainty in the ratio measurement, although this is minimized by employing a very loose cut. Based on existing models for the deuteron, it is assumed that corrections due to the deuteron wave function will diminish with increasing Q^2, and that they provide a negligible error. While the neutron charge form factor enters in this ratio, the uncertainty due to this term becomes small as Q^2 increases and this has little impact on the experimental uncertainties. High-quality data for the proton form factors is necessary for the extraction of the neutron magnetic form factor. The measurement of these quantities is covered elsewhere in this document.

A calculation of the potential coverage in Q^2 and the estimated errors is shown in Fig. 3. There are a number of assumptions which went into this calculation. A luminosity of $2 \times 10^{34} cm^{-2} s^{-1}$ for 30 days was assumed, and the statistical error was calculated using the dipole approximation. While this exceeds the present luminosity limits of CLAS, the upgraded CLAS is planned to include significant improvements in this limit. It should be noted that use of the dipole approximation is likely to be optimistic, so even greater luminosity would be of benefit. An indication of the possible systematic error is given by the solid lines. With further study, this error is likely to decrease. The error bars show statistical errors only. The target location was assumed to be the current CLAS center. Here the beam energy was taken to be 10 GeV. Higher beam energies could be used to achieve even higher values of Q^2, however, suppression of inelastic background would become more problematic and further detailed simulations are required to carry out a proper feasibility study.

As may be seen in the plot, under these assumptions, the neutron elastic

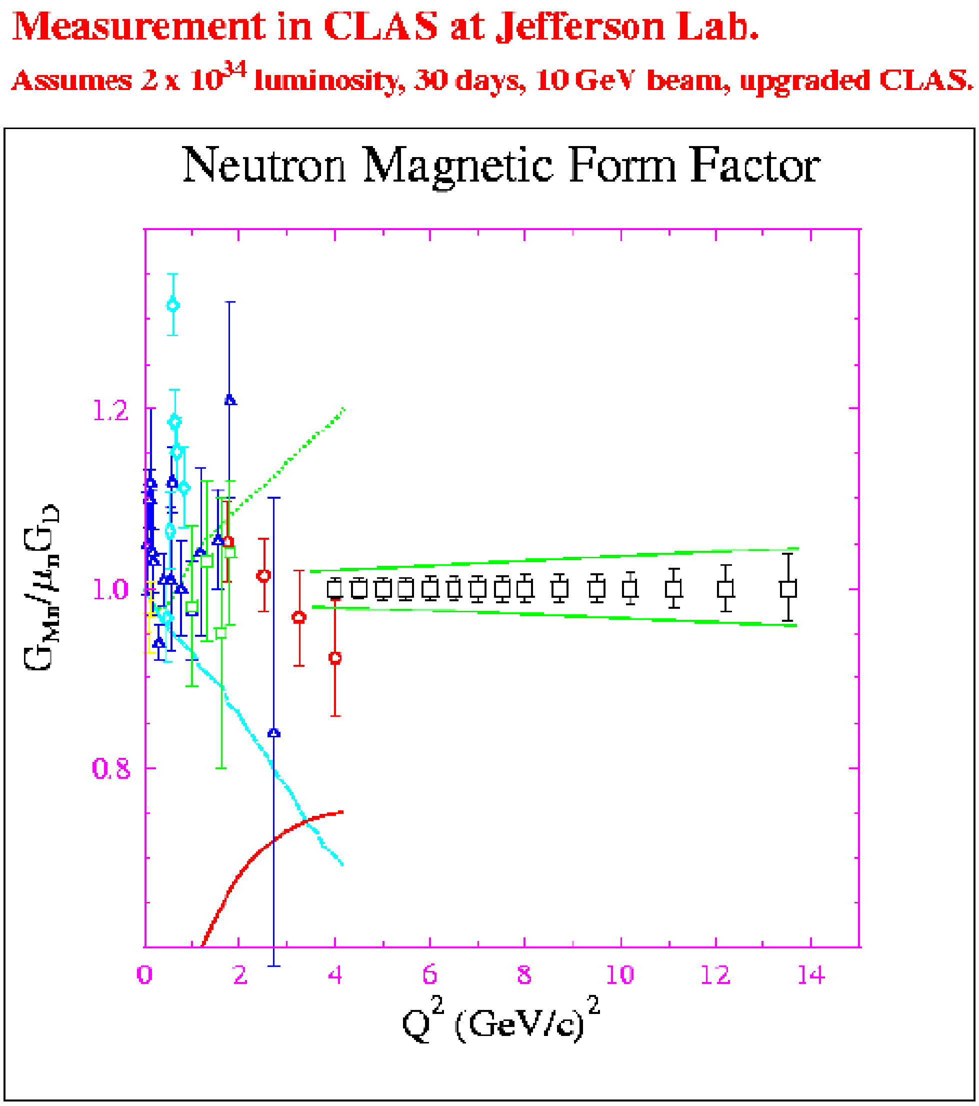

Figure 3: Predicted statistical and systematic uncertainties versus Q^2 for these proposed measurements of G_M^n, contrasted with previous data.

form factor measurement can be extended out to nearly 14 GeV^2, more than tripling the range of the current world data, shown on the left side of the plot. The low-Q^2 portion of the measurement allows adequate overlap both with the published SLAC data (the four highest Q^2 points) and the new data from CLAS. Precision data in this range will have a tremendous impact on our understanding of quark currents in the neutron system.

3.4 Resonance transition form factors

As indicated above, the baryon resonance transition amplitudes are appropriate testing grounds for theoretical approaches to exclusive reactions at different Q^2 regimes. The various versions of the CQM's, GPD's, and *valence* pQCD make very different predictions about the magnitudes, the Q^2 evolution, and the relationships between the contributing helicity amplitudes.

In the CQM the $N \to \Delta(1232)$ transition corresponds primarily to a single quark spin-flip (Fig. 4 - top diagram). This is nearly completely due to an $M1$ electromagnetic multipole, which has a large helicity non-conserving component, as $M1 = -\frac{1}{2}(A_{1/2} - \sqrt{3}A_{3/2})$, where $A_{1/2}$ and $A_{3/2}$ are helicity conserving and non-conserving amplitudes, respectively. This is well borne out by experiments at low Q^2. Alternatively, at asymptotically high Q^2 (Fig. 4 - bottom diagram) valance pQCD predicts $1/Q^4$ scaling for the leading helicity conserving form factors, and $1/Q^5$ ($1/Q^6$) dependence for longitudinal (transverse) next-to-leading order helicity *non*-conserving form factors. In term of multipoles, the vanishing of $A_{3/2}$ relative to $A_{1/2}$ implies $E2 = +M1$ since $A_{3/2} = (M1 - E2)$. Of course at intermediate Q^2, say in the several GeV^2/c^2 range, we should expect a smoothly increasing $E2/M1$ ($\equiv R_{EM}$) ratio, schematically shown in 5, as *hard* processes begin to play a role.

Measurements of the Q^2 dependence of the contributing multipoles (or equivalently helicity amplitudes) of the $N \to \Delta(1232)$ transition should give direct information about the evolution of applicable theoretical descriptions. JLAB Experiment 94-014 [29] in Hall C measured R_{EM} to a maximum Q^2 of 4 GeV^2/c^2, and found R_{EM} remains very small. Where we are on the curve of Fig. 5 is unknown. All we can say is we are somewhere to the left of the rise. At Q^2= 4 GeV^2/c^2 the characteristic wavelength of the probe is $\sim$ 0.1 fm, which should be small enough to begin to probe the short range correlations inherent in the nucleon's structure. Thus, it is fairly safe to assume that R_{EM} will begin to show a deviation from the low Q^2 values, signaling the

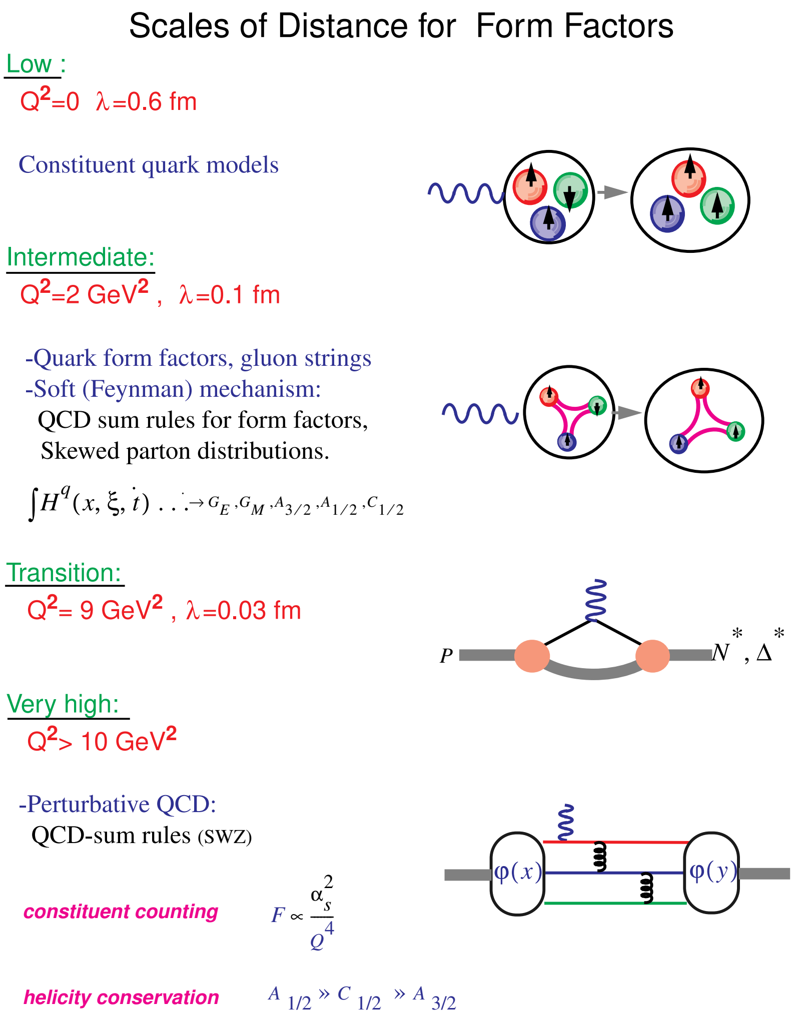

Figure 4: Models for describing baryon form factors at low, medium and high momentum transfer, respectively.

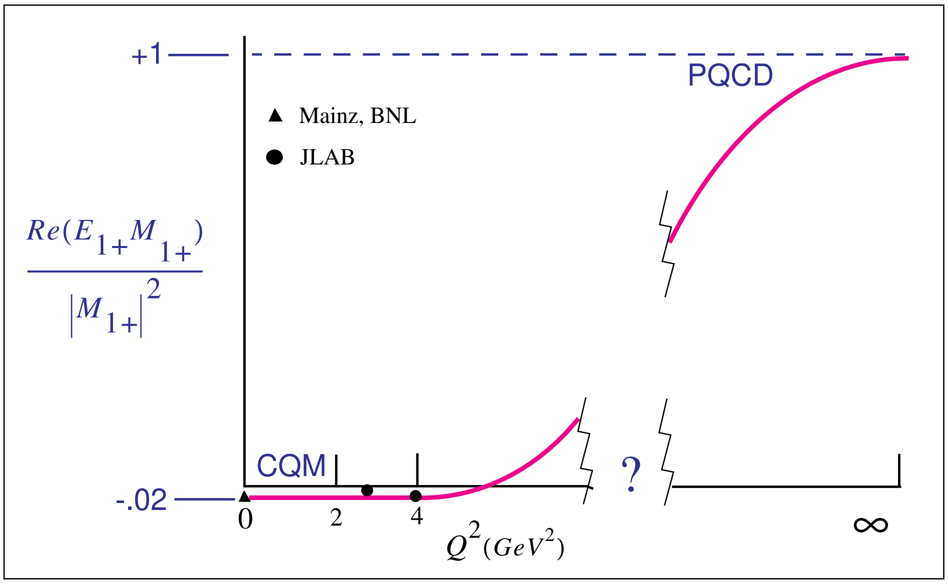

Figure 5: $Re(E_{1+}^{*}M_{1+})/|M_{1+}|^2$ as a function of Q^2. The datum at Q^2=0, is the result of experiments at Mainz and BNL. The data points at Q^2=2.8 and 4 GeV^2/c^2 are the JLAB results. The unmodified SU(6) value is 0, while the PQCD prediction is +1. The curve is a suggestion of what may be expected. The break in the abscissa and the curve indicates our lack of knowledge about where in Q^2 the transition to *hard* processes occurs.

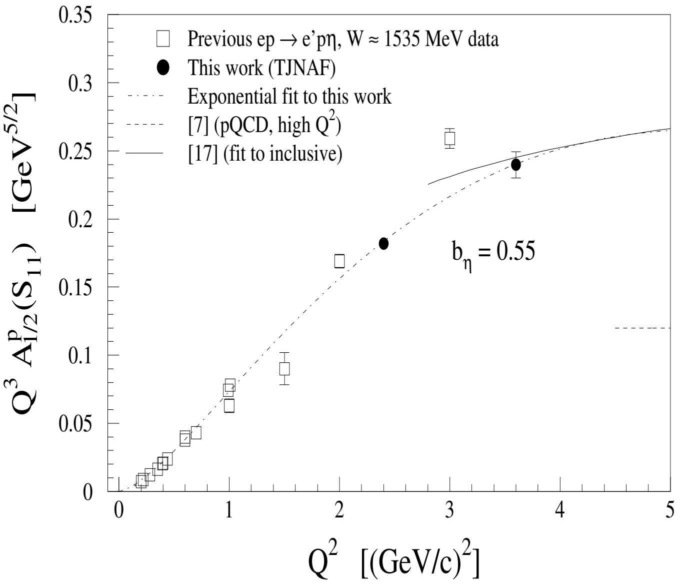

Figure 6: The quantity $Q^3 A^p_{1/2}(Q^2)$ for the $S_{11}(1535)$. The dot-dashed line is an exponential fit to the TJNAF cross section given by the two points at 2.4 and 3.6 GeV^2/c^2, ($\sigma_{res} = 16.5 \exp\left[-0.565\, Q^2\right]$ μb, where Q^2 is in $[(\mathrm{GeV}/c)^2]$), and the solid line is a fit to inclusive data.

onset of *hard* processes.

E94-014 also studied the transition to the $S_{11}(1535)$ excited nucleon state. This state is easily isolated from other resonances since it is the strongest excitation of any resonance at high Q^2, and it is the only major state which de-excites by emission of an η meson. Identification of a single η meson in the final state virtually isolates the $S_{11}(1535)$. Since the $S_{11}(1535)$ has $J^\pi = 1/2^-$ it is only excited by the helicity conserving $A_{1/2}$ amplitude. Therefore this experiment is a very important test case for the onset of hard processes. As with the nucleon and $\Delta(1232)$ it is the lowest lying state with its quantum numbers, so that the amplitude can be calculated using PQCD sum-rule and/or GPD techniques to observe the interplay between soft and hard processes. Fig. 6 shows the current status of the world data including that of experiment 94-014. It can be seen that even at $Q^2 = 3.6$ GeV^2/c^2 the $1/Q^4$ scaling is not yet evident, but there may be a suggestion of its onset.

3.4.1 Proposed Experimental Program.

We propose to measure the evolution of the $\Delta(1232)$ and $S_{11}(1535)$ resonance transition amplitudes to a maximum $Q^2 \sim 15$ GeV^2/c^2. This Q^2 range will allow us to observe the onset of *hard*-correlated processes, and their interplay with the *soft* mechanisms. The measurements will be carried out in Halls B and C. In Hall B the large acceptance of the upgraded CLAS detector will enable us to measure the complete angular distributions of the charged meson decays of these resonances over a large range of Q^2, all simultaneously. In Hall C the high luminosity coupled with high momentum and high resolution of the HMS and proposed SHMS spectrometers will allow us to measure the very small cross sections encountered at the very highest Q^2. Thus, the two halls play complementary roles in mapping out the production and decay of these transition amplitudes.

Hall C's unique niche is to measure neutral meson electroproduction at high Q^2. As in experiment 94-014, we will simultaneously measure the resonant amplitudes of the $\Delta(1232)$ and $S_{11}(1535)$ via $e+p \rightarrow \Delta(1232) \rightarrow p+\pi^0$ and $e + p \rightarrow S_{11}(1535) \rightarrow p + \eta$, respectively.

For the single meson decay channel, measuring only one of the decay hadrons completely determines the kinematics of the entire reaction, including the other undetected hadron. In particular, the neutral single meson is identified by the missing mass of the detected proton and electron, and its c.m. kinematics are determined by the by missing momentum. An important property of high Q^2 reactions of which Hall C can take advantage is that the hadronic reaction products are boosted into a narrow cone relative to the momentum transfer, so that large c.m. angular acceptances in θ and ϕ can be obtained with relatively modest angular acceptance spectrometers. This is especially true for the recoil protons in single neutral meson production, ie. in the reactions $p(e, e'p)\pi^0$, and $p(e, e'p)\eta$. The protons emerge in a narrow cone around the momentum transfer $\vec{q}$. For example, if we consider π^0 production at the Δ peak, $W = 1232$ MeV, at $Q^2 = 10$ GeV^2/c^2 the cone half-angle in the lab corresponding to 4π in the c.m. is 2.7° (47 mr). For $\eta's$ at the peak of the $S_{11}(1535)$ resonance the angle is 2.5° (43 mr). With modest solid angle acceptance spectrometers one can obtain almost all of the decay proton cone, and then select the π^0 and η channels by reconstructing their missing mass. The setup for such an experiment is illustrated in Figure 7.

In experiment 94014 the HMS detected the protons with momenta up to about 3.5 GeV/c, and the SOS detected the scattered electrons with a

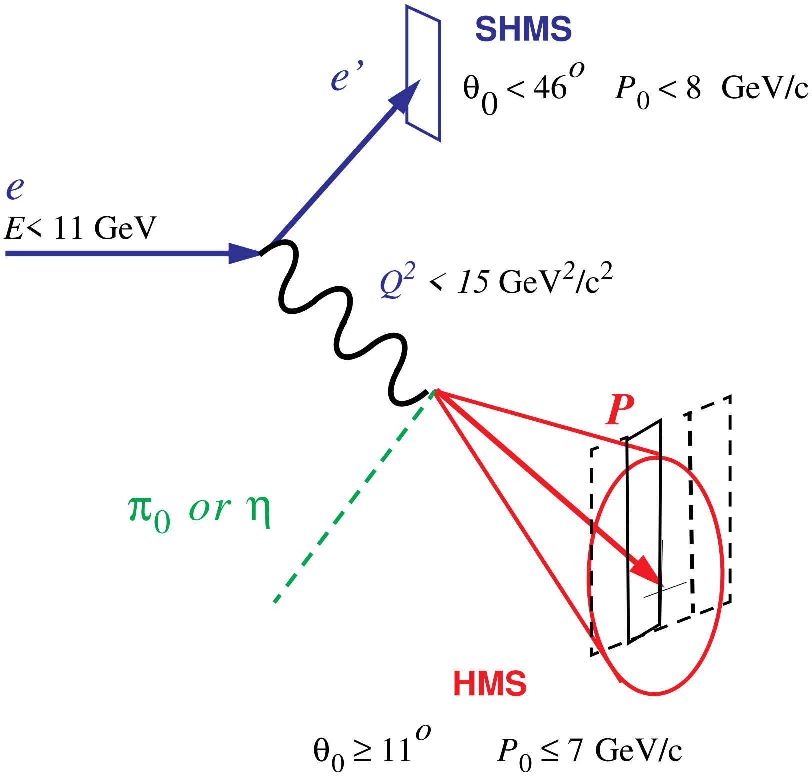

Figure 7: Schematic overview of the experiments $p(e, e'p)\pi^0$ and $p(e, e'p)\eta$ with an electron beam energy 11 GeV and $Q^2 = 10$ GeV^2/c^2. The kinematic requirements for the spectrometers are also indicated.

Table 4: Experimental conditions assumed for the proposed experiment.

Luminosity ($\mathrm{cm}^{-2}\mathrm{s}^{-1}$)	1×10^{38}
Electron (HMS) acceptance $\Delta P_e/P_e \times \Delta\Omega_e$ (msr)	$20\% \times 7$
Proton (SHMS) acceptance $\Delta P_p/P_p \times \Delta\Omega_p$ (msr)	$20\% \times 3$
Momentum resolution (HMS and SHMS) $\delta p/p$	1×10^{-3}
Angular resolution (HMS and SHMS) (rad) $\delta\theta = \delta\phi$	1×10^{-3}

momentum about 1.5 GeV/c. At much higher Q^2 (eg. $\sim$ 15 GeV^2/c^2), the SOS must be replaced by a new spectrometer, putatively SHMS. At these increased Q^2 *both* spectrometers must have high maximum momentum capabilities. In addition *both* must have excellent resolution, as well as large solid angle acceptance. The resolutions in momentum and angle must be excellent because very large Jacobians are involved in transforming the narrow kinematic cone of the detected particles into 4π c.m. Simulations indicate that the measured and proposed spectrometer propoerties allow, e.g., sufficient missing mass resolution over the full kinematics of this proposal.

Large solid angle acceptance is important because the cross sections for resonance production are decreasing rapidly with increasing high momentum transfer. With spectrometers HMS I and HMS II, the Monte Carlo generated angular acceptance in the c.m. is essentially 4π. The η's and π^0's are measured simultaneously in each run.

Table 4 gives the conditions needed to carry out the experiment. Table 5 shows the number of observed S_{11}'s and $\Delta(1232)$'s which would be obtained in 30 day running periods at each Q^2. Projected rates were calculated assuming a dipole fall off of the form factors.

One can see that it is possible to perform a high quality experiment to accurately obtain the dominant multipoles of the $e + p \to \Delta(1232) \to p + \pi^0$ and $e + p \to S_{11}(1535) \to p + \eta$ at a mean Q^2 up to $\sim$ 15. It is made possible only by the unique Hall C capability, including high luminosity coupled with high quality high momentum spectrometers.

3.5 Real Compton Scattering

As indicated above, RCS investigates the $< x^{-1} >$ moments of the GPDs. The ratio of cross sections, $d\sigma/d\sigma_{KN}$, can be used to determine the form factor R_V. The cross section is not very sensitive to R_A, which is best

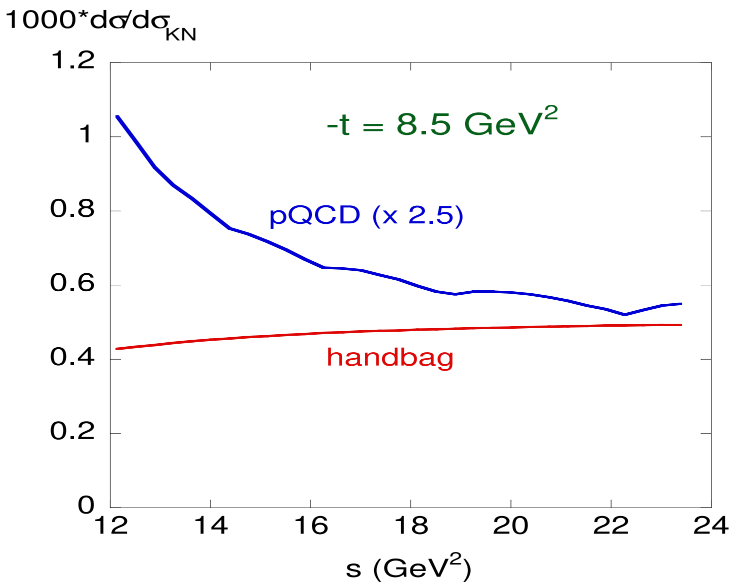

Figure 8: The ratio of RCS to Klein-Nishina cross section.

Table 5: Statistics for $e + p \to \Delta(1232) \to p + \pi^0$ and $e + p \to S_{11}(1535) \to p + \eta$ using HMS and SHMS in Hall C.

Q^2 ($\mathrm{GeV}^2/\mathrm{c}^2$)	Events $S_{11} \to \eta$	Events $\Delta(1232) \to \pi^0$
4	3e+08	1e+08
5	7e+07	3e+07
6	2e+07	1e+07
7	7e+06	3e+06
8	3e+06	1e+06
9	1e+06	5e+05
10	5e+05	2e+05
11	3e+05	1e+05
12	1e+05	6e+04
13	6e+04	3e+04
14	3e+04	1e+04
15	2e+04	7e+03
16	8e+03	4e+03
17	4e+03	2e+03

determined by the longitudinal polarization transfer to the proton. The ratio $d\sigma/d\sigma_{KN}$ at fixed t should be nearly independent of s if the handbag diagram is dominant. An angle-dependent scaling of the cross sections is also expected, with $d\sigma/dt = A(\theta_{cm})/s^n$ and $n > 6$ at angles backward of about 60°. In contrast, pQCD predicts $n = 6$ at all angles. Cross section calculations are shown in Fig. 8 and 9.

Currently E99-114 [30] is an approved initial experimental investigation of RCS, with beam energies of 3 - 6 GeV (s=6.1-11.5 GeV^2). It is intended to measure in the range θ_{cm}=60°-135° (-t up to 6.5 GeV^2). WIth the accelerator upgrade to 11 GeV beam in Halls A and C, the s and $-t$ coverage can be extended to 22 and 12 GeV^2, respectively - see Fig. 10.

3.5.1 Experimental Aspects

At this early stage in the planning process, we propose measurements using the same technique that will be used in E99-114 in Hall A. We present here a summary of the detailed discussion in the proposal. The steup is

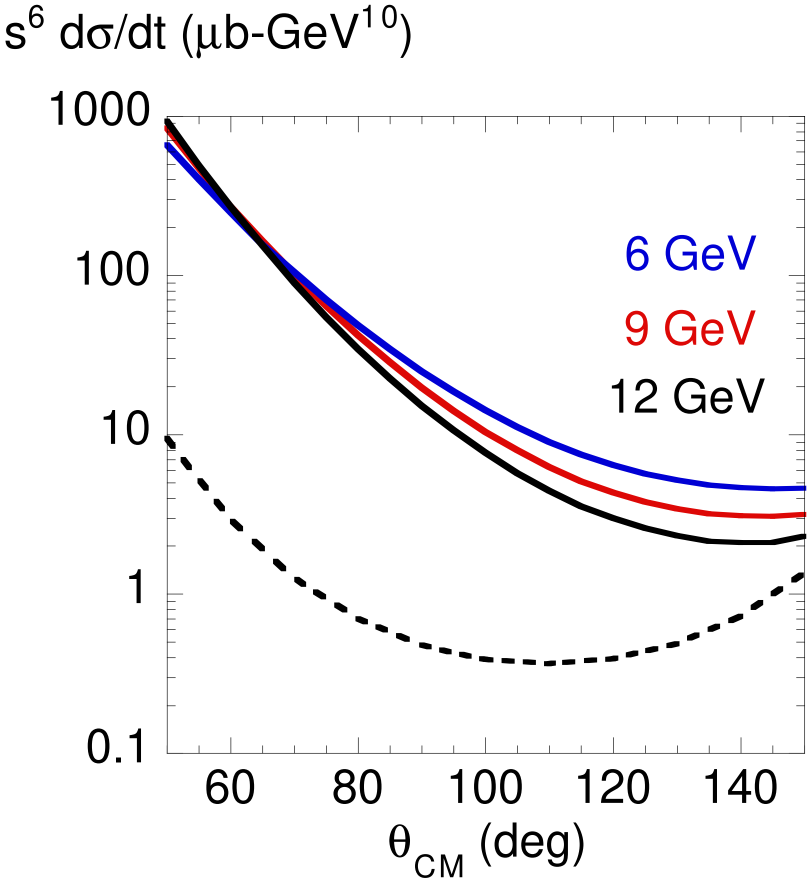

Figure 9: The RCS cross section multiplied by s^6 versus angle and energy. The three solid curves use the handbag mechanism and a model for the form factors. The dashed curve is the pQCD prediction.

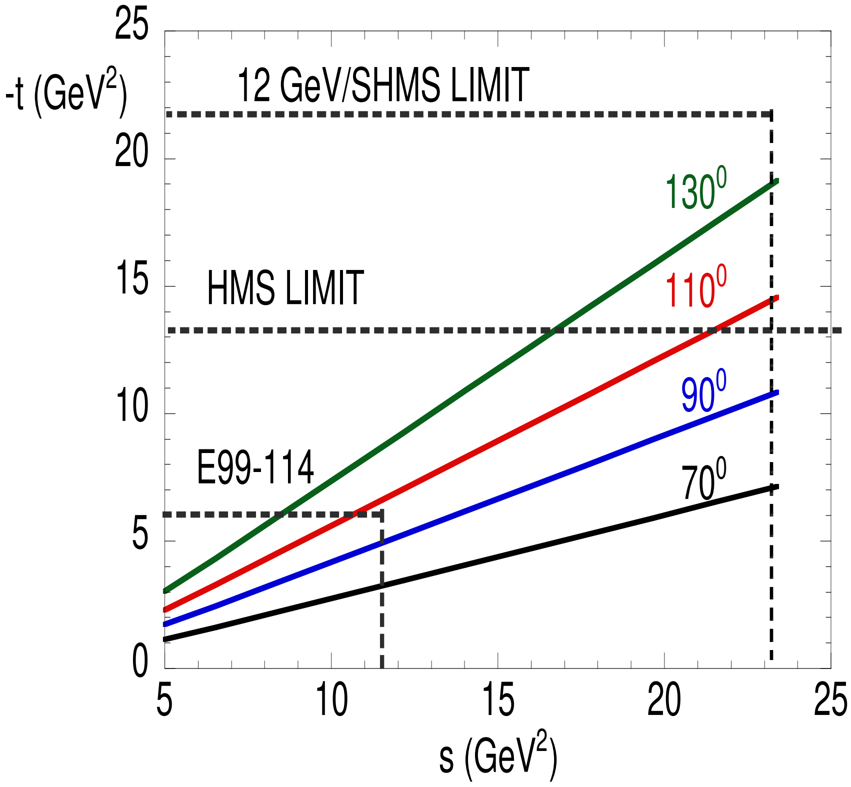

Figure 10: The possible kinematic coverage is shown. The solid diagonal lines are contours of fixed θ_{cm}. The kinematic limits of E99-114, the HMS or proposed MAD, and the proposed SHMS are indicated by horizontal dashed lines. The vertical dashed lines are limits from 6 and 12 GeV beam energies.

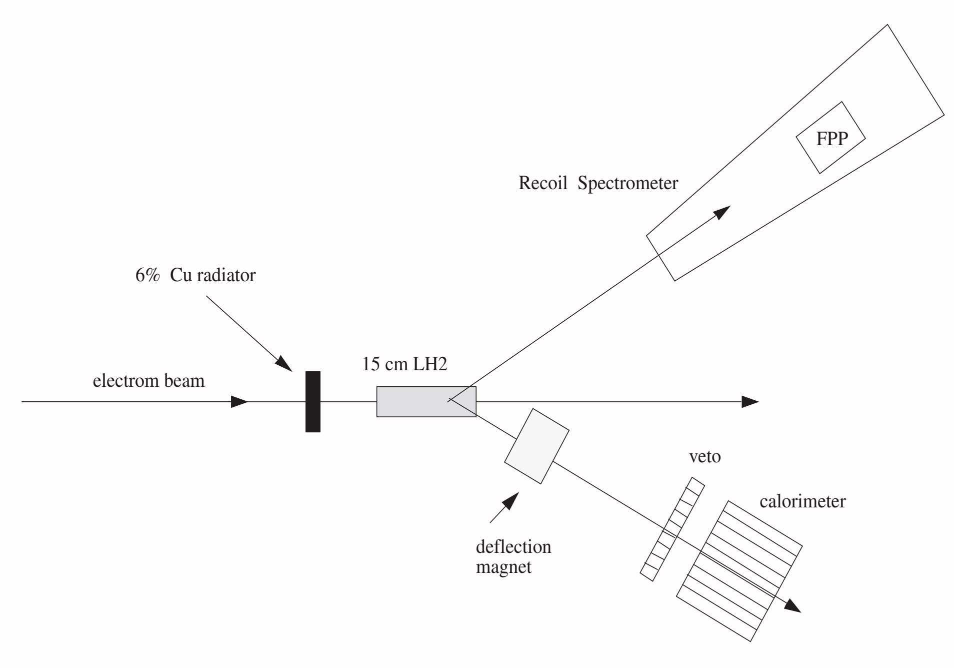

Figure 11: Plan view of the proposed experiment.

shown schematically in Fig. 11. The JLab electron beam is incident on a 6% copper radiator located just upstream of the scattering target. The mixed beam of electrons and bremsstrahlung photons is incident on a 15-cm LH_2 target. For incident photons near the bremsstrahlung endpoint, the recoil proton and scattered photon are detected with high angular precision in a magnetic spectrometer and photon spectrometer, respectively. All measurements proposed herein, for which $-t$ is below 12.5 GeV^2, can be performed in Hall C using the existing HMS, or in Hall A using the proposed MAD. The photon spectrometer, currently under construction for E99-114, is based on a highly segements Pb-Glass calorimeter which covers an area of 1 m^2 and provides a good match in acceptance to the Hall A HRS at lower $-t$. The 2-3 m^2 calorimeter necessary for the G_{Ep} measurement would suffice for the measurements proposed here.

There are two essential features of the experimental technique that deserve comment here. One is the use of the kinematic correlation between

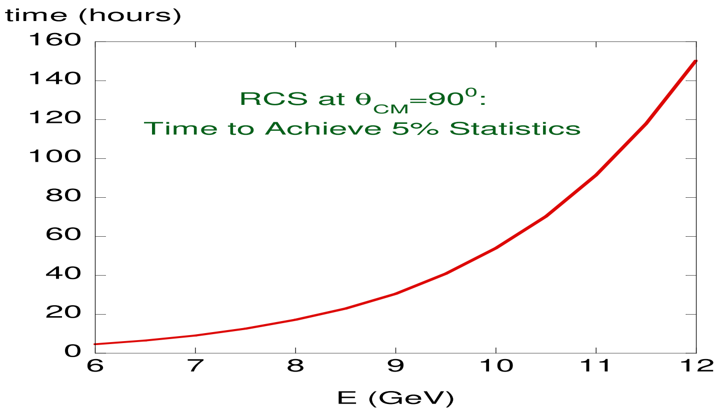

Figure 12: Time needed for the proposed measurements as a function of energy.

the scattered photon and recoil proton in the RCS reaction to reduce the background of π^0 decay photons from the $p(\gamma, \pi^0 p)$ reaction, thereby placing stringent demands on the combined angular resolution of two-spectrometer system. A second essential feature is that a mixed electron-photon beam is used in order to achieve the desired photon luminosity. On the one hand, this introduces the necessity to identify and reject electrons from *ep* elastic scattering, while on the other hand it provides a convenient tool for an *in situ* calibration of the photon spectrometer and normalization of cross sections. Electron identification is achieved by a segmented Lucite Cerenkov veto detector. In addition a magnet between the target and detector deflects the electron by ≥ 10 cm on the front face of the calorimeter, thereby allowing identification by altering the kinematic correlation with the recoil proton relative to undeflected RCS photons.

At this point, it is useful to point out that the luminosity limitation in

E99-114 is expected to come from the high counting rate in the veto detector. A large acceptance chicane that bends the electron beam cleanly around the target and into the beam dump after passing through the radiator would eliminate the need for a veto detector and allow higher luminosities.

We have performed Monte-Carlo calculations at energies up to 12 GeV and concluded that the experiment is feasible over a broad range of kinematics. Generally, the background from π^0 photons is somewhat worse than at 6 GeV but still reasonably manageable. For fixed θ_{cm}, the background from ep events gets progressively worse at the higher energies, due to the ever-decreasing laboratory scattering angle and the sharp forward peaking of the $e-p$ scattering cross section. Finally, the time needed to achieve a given statistical accuracy also dramatically increases at the energy is increased, as shown in Fig. 12.

4 Summary

The nucleon form factors are fundamental quantities that describe one aspect of the internal structure of the nucleon. These quantities test structure models for the nucleon. Specifically, within the frameworks of generalized parton distributions - and of duality - these quantities are related to the deep inelastic structure of the nucleon, and there is promise of a unified picture of nucleon structure. From the perspective of generalized parton distributions, exclusive reactions in general can be considered to measure different moments of the parton distributions, generalizing the concept of form factors. Of particular interest is the possibility to learn about the quark orbital angular momentum contribution to the nucleon spin, and to learn about quark correlations through the large $-t$ behavior.

Precise measurements to date are at low four momentum transfer, below a few GeV^2. With the CEBAF energy upgrade and equipment upgrades in the experimental halls - MAD for Hall A, upgraded CLAS for Hall B, and SHMS for Hall C - a program of precision measurements to $-t$ about 15 GeV^2 becomes possible. The proposed measurements include the elastic form factors G_E^p, G_M^p, and G_M^n, the resonance transition form factors for $p \to \Delta$ and $p \to s_{11}$, and real Compton scattering.

References

[1] R. Hofstadter and R. W. McAllister, Phys. Rev. 98, 183 (1955).

[2] M. K. Jones et al., Phys. Rev. Lett. 84, 1398 (2000).

[3] V. V. Frolov *et al.*, *Phys. Rev. Lett.* **82**, 45 (1999).

[4] G.P. Lepage and S.J. Brodsky, *Phys. Rev.* D **22**, 2157 (1980).

[5] S. Platchkov et al., Nucl. Phys. A510, 740 (1990).

[6] N. Isgur, G. Karl and D.W.L. Sprung, Phys. Rev. D 23, 163 (1981).

[7] A.W. Thomas, Adv. Nucl. Phys. 13, 1 (1984).

[8] X. Ji, *Phys. Rev.* D **55**, 7114 (1997), *Phys. Rev. Lett.* **78**, 610 (1997), J. Phys. G 24, 1181 (1998).

[9] A. Radyushkin, *Phys. Lett.* B **380**, 417 (1996); *ibid.*, *Phys. Lett.* B **385**, 333 (1996); *Phys. Rev.* D **56**, 5524 (1997).

[10] A. Radyushkin, *Phys. Rev.* D **58**, 114008 (1998).

[11] A. Afanasev, E-print: hep-ph/9808291. In: Proc. Workshop on Jefferson Lab Physics and Instrumentation with 6-12-GeV Beams and Beyond, JLab, Eds.: S. Dytman, H. Fenker, P. Roos, p. 263.

[12] A. Afanasev, E-print: hep-ph/9910565. In: Proc. JLab/INT Workshop on Exclusive and Semi-Exclusive Processes at High Momentum Transfer, JLab, May 1999, *to be published*.

[13] M. Boglione, E. Leader, E-print: hep-ph/0005092.

[14] E.D. Bloom and F.J. Gilman, Phys. Rev. Lett. 16, 1140 (1970).

[15] I. Niculescu, Ph.D. thesis, Hampton University, 1999; C. Keppel, talk presented at 7th International Workshop on Deep Inelastic Scattering and QCD (DIS 99), Zeuthen, Germany, Apr. 1999.

[16] A. de Rújula, H. Georgi and H.D. Politzer, Ann. Phys. 103, 315 (1975).

[17] X. Ji and P. Unrau, Phys. Rev. D 52, 72 (1995).

[18] X. Ji and W. Melnitchouk, Phys. Rev. D 56, 1 (1997).

[19] S.D. Drell and T.-M. Yan, Phys. Rev. Lett. 24, 181 (1970).

[20] G.B. West, Phys. Rev. Lett. 24, 181 (1970).

[21] W. Melnitchouk, JLab preprint JLAB-THY-00-08.

[22] C.E. Carlson and N.C. Mukhopadhyay, Phys. Rev. D 58, 094029 (1998).

[23] P. Stoler, Phys. Rep. 226, 103 (1993).

[24] see L. Andivahis *et al.*, Phys. Rev. **D** 50, 5491 (1994) and references therein.

[25] A. F. Sill *et al.*, Phys. Rev. **D** 48, 30 (1993).

[26] P. E. Bosted, Phys. Rev. **C** 51, 409 (1995).

[27] See, e.g., H. Anklin *et al.*, Phys. Lett. **B 336**, 313 (1994); H. Anklin *et al.*, Phys. Lett. **B 428**, 248 (1998); E.E.W. Bruins *et al.*, Phys. Rev. Lett. **75**, 21 (1995); W. Xu *et al.*, to be published.

[28] A. Lung *et al.*, Phys. Rev. Lett. **70**, 718 (1993).

[29] J. Napolitano, P. Stoler *et al.*, CEBAF proposal E94-014; see also C. S. Armstrong *et al.*, Phys. Rev. **D** 60, 052004 (1999).

[30] B. Wojtsekhowski, C. Hyde-Wright, A. Nathan *et al.*, CEBAF proposal E99-114.